ARTICLE

The potential for large-scale CO_2 removal via rock weathering on croplands

David J. Beerling[1]*, Euripides P. Kantzas[1], Mark R. Lomas[1], Peter Wade[1], Rafael M. Eufrasio[2], Phil Renforth[3], Binoy Sarkar[4], M. Grace Andrews[5], Rachael H. James[5], Christopher R. Pearce[6], Jean-Francois Mecure[7,8], Hector Pollitt[8,9], Philip B. Holden[10], Neil R. Edwards[8,10], Madhu Khanna[11], Lenny Koh[2], Shaun Quegan[12], Nick F. Pidgeon[13], Ivan A. Janssens[14], James Hansen[15] & Steven A. Banwart[16,17]

[1]Leverhulme Centre for Climate Change Mitigation, Department of Animal and Plant Sciences, University of Sheffield, Sheffield S10 2TN, UK

[2]Advanced Resource Efficiency Centre, Management School, University of Sheffield, Sheffield S10 1FL, UK

[3]School of Engineering and Physical Sciences, Heriot-Watt University, Edinburgh Campus, Edinburgh EH14 4AS, UK

[4]Lancaster Environment Centre, Lancaster University, Lancaster LA1 4YQ

[5]School of Ocean and Earth Science, National Oceanography Centre Southampton, University of Southampton Waterfront Campus, Southampton SO14 3ZH, UK

[6]National Oceanography Centre, European Way, Southampton, SO14 3ZH, UK

[7]Global Systems Institute, Department of Geography, University of Exeter, Exeter, UK

[8]Cambridge Centre for Energy, Environment and Natural Resource Governance, University of Cambridge, Cambridge, CB3 9EP, UK

[9]Cambridge Econometrics Ltd, Covent Garden, Cambridge CB1 2HT, UK

[10]Environment, Earth and Ecosystems, The Open University, Milton Keynes, MK7 6AA, UK

[11]Department of Agricultural and Consumer Economics, Institute for Sustainability, Energy, and Environment, University of Illinois, Urbana, Illinois 61801, USA

[12]Department of Mathematics and Statistics, Hicks Building, University of Sheffield, Sheffield S3 7RH

[13]Understanding Risk Research Group, School of Psychology, Cardiff University and the Leverhulme Centre for Climate Change Mitigation, Cardiff CF10 3AT, UK

[14]Research Group Plants and Ecosystems, University of Antwerp, Belgium

[15]Earth Institute, Columbia University, New York, NY, USA

[16]Global Food and Environment Institute, University of Leeds, Leeds LS2 9JT, UK

[17]School of Earth and Environment, University of Leeds, Leeds LS2 9JT, UK

*e-mail: d.j.beerling@sheffield.ac.uk

Enhanced silicate rock weathering (ERW) deployable via croplands is a prime candidate to be evaluated for atmospheric Carbon Dioxide Removal (CDR), a backstop for human-caused climate change[1]. ERW has potential co-benefits for improved food and soil security and reduced ocean acidification[2-4]. We use an integrated performance modelling approach for an initial techno-economic assessment for 2050, quantifying how CDR potential and costs vary among nations in relation to business-as-usual energy policies and policies consistent with limiting future warming to 2 °C[5]. China, India, the United States and Brazil have large potential to help achieve average global CDR targets of 0.5 to 2 Gt CO_2 yr^{-1} with extraction costs of ~$80-180 t^{-1} CO_2. These targets and costs are robust regardless of future energy policies. Deployment with existing croplands offers opportunities to align agriculture and climate policy. However, success will depend upon overcoming political and social inertia to develop regulatory and incentive frameworks. We discuss the challenges and opportunities of ERW deployment, including the potential for excess industrial silicate materials (basalt mine overburden, concrete, and iron and steel slag) to obviate the need for new mining, as well as uncertainties in soil weathering rates and land-ocean transfer of weathered products.

Failure of the world to curb fossil fuel CO_2 emissions[6], and the inadequacy of planned mitigation measures[7], has been greeted with growing public consternation[8], consistent with the clear intergenerational injustice of human-caused climate change[9]. Even the most ambitious emission phase-outs[9,10] fail to achieve the United Nations Framework Convention on Climate Change Paris Agreement targets for limiting global warming without the help of massive atmospheric Carbon Dioxide Removal (CDR). Extraction goals[1,7,9,10] later this century in most studies are on the order of at least 10 Gt CO_2 yr^{-1}, although projections of rapid technological change[5] suggest a lower requirement of 2-2.5 Gt CO_2 yr^{-1}. This formidable challenge has led to international calls for urgent research into a portfolio of CDR options to understand their feasibility, scope, costs and challenges[11,12].

Our focus is terrestrial enhanced rock weathering (ERW), a CDR strategy based on amending soils with crushed calcium- and magnesium-rich silicate rocks to accelerate CO_2 sequestration[2-4,13-17]. Basalt, an abundant fast-weathering rock with the required mineral chemistry, is a prime target for implementing land-based ERW because of its potential co-benefits for crop production[18] and soil health[2-4]. ERW liberates base cations, generating alkalinity such that atmospheric CO_2 is converted into dissolved inorganic carbon (principally hydrogen carbonate ions; HCO_3^-) that is removed via soil drainage waters. These weathering products are transported via land surface runoff to the oceans with a storage lifetime exceeding 100,000 years[19]. Depending on soil type, atmospheric CO_2-derived dissolved inorganic carbon may also be sequestered through the formation of soil carbonate minerals, which reduces the efficiency of carbon sequestration by ~50%[19]. Logistical infrastructure to apply basaltic rock dust to managed croplands already exists due to the common need to apply crushed limestone to reverse soil acidification from intensive cropping[2-4]. Thus, rapid deployment at large scale appears feasible within decades, with important ancillary benefits including mitigation of ocean acidification[15-18]. Carbon sequestration by ERW on croplands, a biogeochemical CDR option supporting multiple United Nations sustainable development goals and ecosystem services[4,20], and a pragmatic land-use choice to maximise scalability and co-benefits, thus warrants detailed examination.

We constructed a performance model with sub-national level of detail to assess quantitatively the CDR capacity and costs for land-based ERW implementation in major economies, constrained by available agricultural land area and energy production (including

USA, India, China, Brazil, and Europe) (**Extended Data Fig. 1**). For rock weathering within the soil profile, we developed a 1-D vertical reactive transport model with steady-state flow, and a source term representing rock grain dissolution (Methods; SI figs. S1-S12; SI tables S1-S5). Our work builds on advances made in prior ERW research largely on tropical forested ecosystems[15-17,21,22], with the practical aims of understanding the capacity of agriculture to capture carbon via soil amendment with milled basalt. For this initial nation-by-nation assessment, we examine the sensitivity of net CDR with current croplands to projected national energy production for 2050 under a business-as-usual energy (BAU) scenario based on ongoing energy transitions[5]. This is compared with a 2°C scenario, which includes a wide range of policy measures designed to respect the 2°C target with 75% probability[5] (SI tables S6-S12).

Carbon removal potential via ERW

Our geospatial analyses define a new technical potential CDR range for those nations with high capacity for ERW deployment on cropland (**Figure 1**; SI figs. S13-S15). For each nation, we generate CO_2 capture curves by ranking CDR potential from the highest to the lowest grid cells with increasing ERW deployment. National median CO_2 removal curves typically show CDR capacity rising with increasing cropland area, with carbon removal by silicate soil amendment reaching a plateau or declining in the case of Canada (**Figure 1**). These patterns reflect expansion of ERW into climatically unfavourable agricultural land, causing CDR potential to slow relative to the carbon penalty of logistical operations, and the 3% limit in national energy available for grinding (**Extended Data Fig. 2**). Overall trends in national CDR curves are relatively insensitive to the choice of energy scenario. China is the exception because its large increase in low carbon energy usage projected under the 2°C scenario[5] allows net CDR to rise by substantially reducing secondary CO_2 emissions from logistical operations (**Figure 1**). This contrasts with results for India, whose total energy production falls by ~40% with a transition to low carbon energy production in the 2°C scenario, lowering energy available for grinding basalt, and thus the potential for increased CDR by ERW. Reductions in energy production for other nations in the 2°C scenario compared with the BAU scenario similarly lower their potential for increased CDR with the transition to low carbon energy.

Recognising the urgent need to assess large-scale options for meeting near-term CO_2 removal goals[10], we determine the potential contribution of nations to achieve CDR targets across the 0.5-2 Gt CO_2 yr^{-1} range (**Table 1; Extended Data Fig. 3**). Overall, we find the three top ranked countries with the highest CDR potential are coincidentally the highest fossil fuel CO_2 emitters (China, USA and India)[6] (**Figure 1**). Indonesia and Brazil, with CO_2 emissions 10-20 times lower than the USA and China, have relatively high CDR potential due to extensive agricultural lands and climates suitable for high silicate rock weathering efficiency. European countries have an order-of-magnitude lower CDR potential than China, USA, and India, mainly because of lower agricultural land area. The top five European nations with the highest net CDR potential could offset 30% of the EU27's current emissions and the top three European countries with highest CDR potential are also the largest European emitters of CO_2 from fossil fuels (Germany, Spain and Poland)[6]. Our ERW scenarios (**Table 1**) correspond to an aggregate CDR of 25-100 Gt CO_2 if sustained over 5 decades. This would save up to 10% of the remaining cumulative carbon emission budget

(~900 Gt CO_2) that gives a likely chance of limiting global warming to less than 2°C above the pre-industrial average surface temperature[10].

In the context of our CDR targets, ERW has a similar potential to that of other CDR strategies[23] estimated for 2050, including bio-energy with carbon capture and storage (BECCS), widely adopted in IPCC future scenarios (0.5-5 Gt CO_2 yr^{-1}), direct air carbon capture and storage (DAC) (0.5-5 Gt CO_2 yr^{-1}), biochar (0.5 to 2 Gt CO_2 yr^{-1}), soil organic carbon (SOC) sequestration (0.5-5 Gt CO_2 yr^{-1}), and afforestation/reforestation (0.5-3.6 Gt CO_2 yr^{-1}). One benefit of country level analysis for CDR is the scope for comparative assessments with other technologies and opportunities for co-deployment. For example, our ERW CDR range is comparable with large-scale implementation of BECCS in USA by 2040 (0.3-0.6 Gt CO_2 yr^{-1}), as constrained by biomass productivity, location and capacity of CO_2 storage sites[24]. ERW avoids competition for land used in food production, and related increased demands of BECCS for freshwater and polluting fertilizers[25], with CO_2 being treated as a resource for mineral weathering. Co-deployment of ERW with feedstock crops for BECCS and biochar could enhance the feasibility and carbon sequestration potential of these strategies[4,26].

Inorganic carbon sequestration by ERW appears comparable to SOC sequestration, another proposed CDR strategy (~2.5 Gt CO_2 yr^{-1} by 2100)[27] using agricultural land, but with potentially greater long-term security of C-storage. Co-deployment of ERW and SOC sequestration at large-scale might, therefore, contribute substantially to the 5 Gt CO_2 yr^{-1} carbon removal target suggested in decarbonization scenarios[10] for 2050. Compatibility of ERW and SOC sequestration may be realistic given that amendment of acidic organic-rich soils with silicate minerals, and resultant pH increase, had no effect on respiratory CO_2 fluxes[28,29], contrary to concerns that increased soil pH may accelerate organic matter decomposition[30]. However, efficacy of CO_2 removal, sink saturation, and permanency of storage with these approaches, separately and interactively, are uncertain[11,23]. Abatement of soil N_2O emissions by basalt application to conventionally managed arable and perennial crops[31], and of N_2O and CH_4 emissions by application of artificial silicates to rice agriculture[32], is possible. Such effects would further lower adverse impacts of agriculture on climate per unit yield, amplifying the climate mitigation potential of ERW.

Greenhouse gas emissions reductions aimed at limiting future warming are defined under the Paris Agreement by Nationally Determined Contributions (NDCs)[33]. As yet, most of the top 10 fossil carbon emitting nations are failing to meet their 2030 NDC pledges which, even if met, imply a median warming (2.6–3.1 °C) exceeding the Paris agreement[33]. Warming of this magnitude could allow the Earth system to cross thresholds for irreversible planetary heating and long-term multi-metre sea-level rise, with potentially disastrous consequences for coastal cities[34]. NDC pledged carbon emission reductions undergo periodic revision in response to trends in greenhouse gas emissions, uptake of low-carbon energy technology, and climate[33] and hence are not set for 2050. We therefore illustrate the potential for undertaking ERW with agricultural lands to strengthen near-term national 2030 NDCs (**Figure 2**).

Results show that China may be able to augment its pledged 2030 NDCs by ~5-10%, with similar gains for the USA, which has opted-out of the Paris agreement. For India, the gain rises to 40% of its current pledged emissions, and Brazil may be able to offset 100% of its pledged 2030 CO_2 emissions plus some fraction of those from other countries (**Figure 2**). Other countries outside Europe considered in our analysis (Indonesia, Canada, Mexico) may be able to augment their NDCs by up to 30% (**Figure 2**). In Europe, ERW could aid

significant decarbonisation of France and Spain (up to approximately 40%), and to a lesser extent Poland, Italy and Germany (all ~10%) (**Figure 2**). ERW, therefore, has a role to play in compensating for residual carbon emissions from sectors recognized as being difficult to decarbonize, e.g., transportation by aviation, shipping, and agriculture[1,11].

Costs of carbon removal via ERW

Cost assessment is needed to evaluate commercial feasibility of ERW and to put a price on climate mitigation actions (**Extended Data Fig. 4)**. Our cost estimates based on current prices fall within the range of prior ERW assessments ($75-250 tCO_2^{-1})[21-23] while resolving differences among nations (**Figure 3; Table 1;** SI figs. S16-S25; SI tables S13-S14). Average costs in USA ($160-180 t^{-1} CO_2), Canada and European nations ($160-190 t^{-1} CO_2) are almost 50% higher than those in China, India, Mexico, Indonesia, and Brazil ($55-120 t^{-1} CO_2). The difference largely reflects labour, diesel and electricity costs.

Defined as the cost of CO_2 removal and storage, the price of carbon is a proposed economic enabler for bringing CDR strategies to market[11]. Carbon price is forecast by the World Bank[11] to reach $100-150 t^{-1} CO_2 by 2050. Costs per t CO_2 removed are generally within this projected carbon price range in all nations, but unit costs increase when cropland area exceeds the optimal fraction, because the efficiency of weathering and CDR falls (**Figure 3; Table 1**). A carbon price of $100-150 t^{-1} CO_2 would cover most of the ERW costs for the key nations reported here. It would make ERW an economically attractive option for fast-growing nations, such as India, China, Indonesia, Brazil and Mexico given their estimated CO_2 extraction costs of ~ $75-100 t^{-1} CO_2 (**Figure 3**).

Our estimated ERW costs of carbon removal for nations are comparable to estimates summarized for BECCS ($100 to 200 t^{-1} CO_2), DAC ($100-300 t^{-1} CO_2), and biochar ($30–$120 t^{-1} CO_2), but higher than estimates for SOC sequestration ($0-10 t^{-1} CO_2)[23]. Afforestation/reforestation and practices that increase soil carbon in natural ecosystems, including wetland restoration, have lower estimated costs (<$100 t^{-1} CO_2)[23]. These options, like ERW, require assessment of possible indirect unintended positive climate feedbacks.

Per capita metrics help conceptualize the matter of costs in terms relevant to citizens. Current fossil fuel emissions per person per year[6] are 16.5 t CO_2 (USA), 15.1 t CO_2 (Canada), 7.5 t CO_2 (China), 7.3 t CO_2 (EU28), 2.6 t CO_2 (Brazil), 1.8 t CO_2 (Indonesia) and 1.7 t CO_2 (India). ERW cannot offset all fossil fuel emissions, but using its cost as a guide, the per capita annual cost of achieving zero net emissions, a goal for decarbonisation, would be highest for Canada ($3004), the USA ($2780), China ($832) and EU28 nations ($1288). Costs fall substantially for citizens in Brazil ($300), Indonesia ($103) and India ($135) (**Table 1**).

At this early stage of research and development, costs are uncertain and in need of demonstration projects[7,11,12]. Costs will likely decline as the market expands and technologies develop. This includes emergence of more energy-efficient, low-carbon technologies for rock grinding. Costs may also decline via co-deployment with afforestation/reforestation projects or agroforestry as part of worldwide carbon-offset trading schemes[7]. Net cost of ERW may be lower if rock dust is used as a fertilizer in organic agriculture, which currently occupies 57.8 million hectares, because it adds economic value by improving soil health, fertility and ecosystem services[35].

Implementation challenges and opportunities

Our analysis of the techno-economic potential for CDR via ERW strengthens the case for evaluating all aspects of practical deployment in developed and developing economies. This includes meeting rock demand through alternative sources that avoid mining expansion, widening to more complete economic valuation, through to public perception and social acceptance.

National demand for crushed silicate rock is contingent on extent of ERW deployment (**Extended Data Fig. 5)**. Within our scenarios, the demand for basalt required for ERW rises with an increasing CDR target and scales with agricultural land area (**Table 1**). Safeguarding against substantial increased mining and possible adverse impacts on livelihoods[36], requires exploiting underutilized stockpiles of crushed basalt produced as a by-product of the aggregate industry. Mining generates a continuous but usually discarded finely powered silicate by-product utilizable for ERW without embodied CO_2 emissions that reduce CDR efficiency (**Extended Data Fig. 6**)[21-23], and which has been accumulating worldwide for decades. However, national inventories of the location, availability and extent of this resource are required to assess the potential contribution of this resource to carbon removal.

Requirement for mining may be further reduced by utilizing artificial silicate by-products from industrial processes[37,38], including calcium-rich silicates produced by iron and steel manufacturing (slags) with a long history of agricultural usage[4,39]. This material is recycled as low value aggregate (~<\$5 t^{-1}), and often stockpiled at production sites or disposed of in landfills, whereas it could become a valuable commodity for CDR. The largest amounts of by-products from the construction and demolition industry are cement, sand, and masonry. Following separation from other materials (e.g., metals and plastics), the cement comprises relatively 'clean' calcium-rich silicates and may be suitable for application to soils, but this suggestion requires field trials to assess suitability. Cement contributes ~6% to global CO_2 emissions[6] and ERW may represent a land management option for valorising by-products to capture carbon and improve the sustainability of this worldwide industry.

We forecast production of artificial calcium-rich cements for construction and by-product slag from steel manufacturing for Brazil, China, India, and the USA, to understand their potential role in meeting silicate demand for ERW (**Figure 4**). Differences between national production estimates are driven by forecast population increases over the coming century, and per capita consumption trends for the material under the middle-of-the-road Shared Socioeconomic Pathway (Methods). Bulk silicate production, linked to the construction and demolition sector, is modelled to increase substantially in all four nations, with China and India having combined production by 2060 of ~13 Gt yr^{-1} (**Figure 4**). China and India dominate with above-average per capita cement consumption compared to the global average, and substantially larger populations than the USA and Brazil[38]. Thus, bulk silicate production of these two nations could meet the demand for ERW with large CDR potential (**Table 1**). Although chemically similar to basalt, these artificial calcium-rich silicates contain minerals that dissolve several orders of magnitude faster, react rapidly with CO_2 in soils under ambient conditions[40], and are produced in fine particle sizes that facilitate accelerated weathering[41].

Agricultural production can benefit substantially from increased resource use efficiency, reducing consumption of raw materials and recovering mineral nutrients from silicate by-products[32,42,43], and overburden legacy reserves[44]. However, application of any silicate material to agricultural soils requires careful assessment of the risks including potential release of metals and persistent organic compounds (SI table S15). Undertaking

ERW practices with these materials addresses a critical need to fertilise soils with silica and other nutrients lost by harvesting that gradually depletes plant-available pools[39]. Intensification of food production across 24 million hectares of productive agricultural land in South Asia and China, for example, is creating acidified, desilicated soils exhausted in plant nutrients (potassium, zinc and available phosphorus) that limit yields[45]. Yet these negative effects may be reversible with ERW treatments given fertilization of irrigated rice using either natural and/or artificial silicates (e.g., recycled steel slags) replenishing plant available silica pools, increasing yields and soil pH, and decreasing the mobility of potentially toxic trace elements (e.g., arsenic)[46]. ERW may therefore also have a role in remediation of toxic metal contaminated soils and sediments across 20 million hectares of cultivated land in southern China and elsewhere[47].

More broadly, innovative ERW practices via soil amendments with targeted silicate minerals could help rebuild rapidly deteriorating agricultural soils on which over six billion people depend directly for food[48]. Such practices may complement other approaches to soil improvement, including conservation tillage and nitrogen-fixing cover crops. The current substantial rate of agricultural top-soil depletion requires urgent remedial action, with significant economic costs apparent already in China where degradation of soils supporting wheat, maize and rice production costs an estimated $12 billion annually[48]. Targeted amendment of agricultural soils for CO_2 removal may have a role in slowing rates of soil loss by up to 45%, with the accelerated weathering of added minerals replacing inorganic nutrients and resultant formation of clays and mineral organic aggregates increasing the cation exchange capacity and water storage capacity of rebuilt soils[4,20]. Addition of trace amounts of zinc and iron could also improve public health by reversing the effect of rising CO_2 levels on the declining nutritional value of food crops[49].

Feasibility of mobilizing millions of smallholder communities to adopt ERW practices in China and India will depend on demonstrating soil improvements can reverse yield declines, and on government subsidies. Farming practices adopted for increasing sustainable productivity, for example, have transformed agriculture across 37 million hectares in China, increasing profits by $12.2 billion over a decade[50]. With 2.5 billion smallholders farming 60% of the world's arable land, a similar outreach programme could be used throughout Asia, with farmers earning more profits from higher yields while sequestering CO_2. Involving local scientists in conducting research into its effectiveness and safety to build trust and engagement with smallholder farmers is key, alongside involvement with policymakers and stakeholders. This increases the potential to bring smallholders out of extreme poverty and, in the regions with climates suitable for non-irrigated agriculture, restore highly degraded soils not suitable currently for food production.

Realizing the potential of ERW as a biogeochemical approach to sequester CO_2 by altering land management practices will depend on the commitment of farmers and governments, implementation of the right policy frameworks, and wider public acceptance. Understanding the balance between positive and negative outcomes in terms of public acceptance of the inevitable trade-offs between local mining activities versus global sequestered carbon, requires empirical testing with stakeholders and the wider public. Crucially, such testing needs to understand the conditions that society might place upon the development and large-scale deployment of ERW technologies, as part of a wider responsible research and innovation programme[51].

Uncertainties

Our analysis of the techno-economic potential of CDR by ERW is subject to several uncertainties, particularly variation in our baseline application rate and basalt mineralogy. It also identifies priority areas benefitting from more research of ERW under field conditions.

Extrapolation of laboratory weathering rates to the field scale is a recognized potential source of uncertainty in calculated CDR rates by ERW[2-4,22-24]. We addressed this by Monte Carlo analysis of the fractal dimension accounting for uncertainty in the apparent reacting surface area of grains for ERW conducted at large geographical scales. Together with the chemical affinity effects accounted for in our model, we constrain some of the systematic errors embedded in prior ERW assessments[15-17,21,22].

Surface passivation, a component of chemical inhibition, occurs as weathering proceeds, creating leached layers and relatively stable secondary minerals, which potentially inhibit the mass transfer kinetics of elements from the dissolving surfaces of primary minerals. Current state-of-knowledge[52] precludes a detailed treatment of the role of surface passivation by formation of amorphous silica-rich surfaces for basalt grains added to agricultural soils. ERW analysis will benefit from future research to improve mechanistic insight and formulation of kinetic equations.

It remains to be determined if our theoretical analyses of the techno-economic potential for this CDR approach are consistent with findings from long-term field-scale ERW trials. Such trials are urgently required to assess weathering and CO_2 removal efficiency of freshly crushed rock grains with highly reactive surfaces added to agricultural soils subject to periodic wet-dry cycles during the growing seaon[3]. The potential for trapping of weathered cations on ion exchange surfaces or within secondary minerals other than carbonates delaying, or even preventing, land-ocean transfer will depend on soil type, climate, hydrological conditions, application rate and management practices. Duration of carbon sequestration rate, and possibility for CO_2 sink saturation with ERW on croplands, are both poorly constrained by data, in common with other land-based CDR strategies[11,23], and affect cumulative CDR potential in coming decades. Other areas for further research include quantification of biogeochemical transformations of carbon and nitrogen associated with organic and inorganic fertilization practices, atmospheric deposition, and the role of rhizosphere biology.

Conclusions

Techno-economic assessment of ERW's potential to contribute large-scale CDR requires further integration of nation-by-nation quantitative analysis together with large-scale pilot demonstrators supported by fundamental process studies and public engagement. Our analysis identifies engineering challenges if ERW were to be scaled-up to help meet ambitious CDR targets as part of a wider portfolio of options[1,7,11,12]. ERW estimated costs are comparable to current estimates for the intensive carbon removal technologies, BECCS and DAC, and with potential for ancillary benefits by limiting coastal zone acidification and improving food and soil security. Nations that may have large ERW potential, including China, the United States and India, are all vulnerable to climate change and resultant sea-level rise[34]. Their high risks of economic damage[53] and social disruption provide impetus for creative co-design of agricultural and climate policies. Success requires incentives and regulatory frameworks that overcome social and political inertia. Silicate demand of nations must also be met in a way that facilitates social acceptance[51,54] and preservation of biodiversity[4,20].

Deployment of any CDR strategy is inhibited by concern that it may erode society's perception of the climate threat and the urgency of mitigation measures[54]. The ancillary benefits of ERW may aid its early use and relieve such concern. Innovative 'climate-smart' farming practices can be designed with ERW to draw down CO_2 and other greenhouse gases while recycling nutrients, aiding soil water storage, and supporting crop production[4,18,20]. Such practices can help restore deteriorating top-soils that underpin food security for billions of people while maximizing societal co-benefits needed to incentivise deployment[20]. Financial, industrial and policy road-mapping that links short-term and long-term goals is needed, including a broader analysis of risks[23] and co-benefits[2-4,18,20], to determine the role that ERW might play in climate risk mitigation.

Online content

Any methods, additional references, Nature Research reporting summaries, source data, extended data, Supplementary Information, acknowledgements, peer review information; details of author contributions and competing interests; and statements of data and code availability are available at ….

1. Intergovernmental Panel on Climate Change (IPCC). *Global warming of 1.5°C. An IPCC Special Report on the impacts of global warming of 1.5°C above pre-industrial levels and related global greenhouse gas emission pathways* (World Meteorological Organization, Geneva, Switzerland, 2018).
2. Kantola, I.B. *et al.* Potential of global croplands and bioenergy crops for climate change mitigation through deployment for enhanced weathering. *Biol. Lett.* **13**, 20160714 (2017).
3. Zhang, G., Kang, J., Wang, T. & Zhu, C. Review and outlook for agromineral research in agriculture and climate change mitigation. *Soil Res.* **56,** 113-122 (2017).
4. Beerling, D.J. *et al.* Farming with crops and rocks to address global climate, food and soil security. *Nat. Plants* **4,** 138-147 (2018).
5. Mercure, J.-F. *et al.* Macroeconomic impact of stranded fossil fuel assests. *Nature Clim Change* **8,** 588-593 (2018).
6. Le Quéré, C. *et al.* Global carbon budget 2018. *Earth Syst. Sci. Data* **10**, 1-54 (2018).
7. United Nations Environment Programme. *The Emissions Gap Report 2018* (United Nations Environment Programme, 2018).
8. Hagedorn, G. *et al.* Concerns of young protester are justified. *Science* **364,** 139-140 (2019).
9. Hansen, J. *et al.* Young people's burden: requirement of negative CO_2 emissions. *Earth Sys. Dyn*. **8,** 577–616 (2017).
10. Rockström, J. *et al.* A roadmap for rapid decarbonisation. *Science* **355,** 1269-1271 (2017).
11. The Royal Society. *Greenhouse gas removal technologies* (The Royal Society, London, 2018).
12. Pacala, S. *et al. Negative emissions technologies and reliable sequestration* (National Academy of Sciences, Washington, USA, 2018).
13. Seifritz, W. CO_2 disposal by means of silicates. *Nature* **345,** 486 (1990).
14. Schuiling, R. D. & Krijgsman, P. Enhanced weathering: an effective and cheap tool to sequester CO_2. *Clim. Change* **74**, 349–354 (2006).
15. Kohler, P., Hartman, J. & Wolf-Gladrow, D.A. Geoengineering potential of artificially enhanced silicate weathering of olivine. *Proc. Natl Acad. Sci. USA* **107**, 20228–20233 (2010).
16. Hartmann, J. *et al.* Enhanced chemical weathering as a geoengineering strategy to reduce atmospheric carbon dioxide, supply nutrients, and mitigate ocean acidification. *Rev. Geophys.* **51**, 113–149 (2013).
17. Taylor, L.L. *et al.* Enhanced weathering strategies for stabilizing climate and averting ocean acidification. *Nat. Clim. Change* **6**, 402–406 (2016).

18. Kelland, M.E. *et al.* Increased yield and CO_2 sequestration potential with the C_4 cereal crop *Sorghum bicolor* cultivated in basaltic rock dust amended agricultural soil. *Global Chang. Biol.* doi: 10.1111/gcb.15089, in the press (2020).
19. Renforth, P. & Henderson, G. Assessing ocean alkalinity for carbon sequestration. *Rev. Geophys.* **55**, 636–674 (2017).
20. Smith, P. *et al.* Land-based options for greenhouse gas removal and their impacts on ecosystem services and the sustainable development goals. *Annu. Rev. Environ. Resour* **44,** 255-286 (2019).
21. Renforth, P. The potential of enhanced weathering in the UK. *Int. J. G. Gas. Cont.* **10**, 229–243 (2012).
22. Strefler, J. *et al.* Potential and costs of carbon dioxide removal by enhanced weathering of rocks. *Environ. Res. Lett.* **13,** 034010 (2018).
23. Fuss, S. *et al.* Negative emissions – part 2: costs, potentials and side effects. *Environ. Res. Lett.*, **13,** 063002 (2018).
24. Baik, E. *et al.* Geospatial analysis of near-term potential for carbon-negative bioenergy in the United States. *Proc. Natl Acad. Sci. USA*, **115,** 3290-3296 (2018).
25. Heck, V., Gerten, D., Lucht, W. & Popp, A. Biomass-based negative emissions difficult to reconcile with planetary boundaries. *Nat. Clim. Change* **8,** 151-155 (2018).
26. Amann, T. & Hartmann, J. Ideas and perspectives: synergies from co-deployment of negative emissions technologies. *Biogeosciences*, **16,** 2949-2960 (2019).
27. Mayer, A., *et al.* The potential of agricultural land management to contribute to lower global surface temperature. *Sci. Adv.* **4,** eaaq0932 (2018).
28. Groffman, P. M. *et al.* Calcium additions and microbial nitrogen cycle processes in a northern hardwood forest. *Ecosystems* **9**, 1289–1305 (2006).
29. Dietzen, C., Harrison, R. & Michelsen-Correa, S. Effectiveness of enhanced mineral weathering as a carbon sequestration tool and alternative to agricultural lime: an incubation experiment. *Int. J. Greenhouse G. Cont.* **74,** 251-258 (2018).
30. Smith, P., Haszeldine, R.S. & Smith, S.M. Preliminary assessment of the potential for, and limitations to, terrestrial negative emissions technologies in the UK. *Environ. Sci. Processes Impacts*, **18,** 1400, doi: 10.1039/c6em00386a (2016)
31. DeLucia, E., Kantola, I., Blanc-Betes, E., Bernacchi, C. & Beerling, D.J. Basalt application for carbon sequestration reduces nitrous oxide fluxes from cropland. *Geophys. Res. Abs.*, **21,** EGU2019-4500 (2019).
32. Das, S. *et al.* Cropping with slag to address soil, environment, and food security. *Front. Microbiol.* **10,** article 1320 (2019).
33. Rogelj, J. *et al.* Paris Agreement climate proposals need a boost to keep warming well below 2 °C. *Nature* **534,** 631-639 (2016).
34. Clark, P.U. *et al.* Consequences of twenty-first-century policy for multi-millennial climate and sea-level change. *Nat. Clim. Change* **6,** 360-369 (2016).
35. Crowder, D.W. & Reganold, J.P. Financial competitiveness of organic agriculture on a global scale. *Proc. Natl Acad. Sci. USA* **112,** 7611-7616 (2015).
36. Bebbington, A.J. & Bury, J.T. Institutional challenges for mining and sustainability in Peru. *Proc. Natl Acad. Sci. USA* **106,** 17296-17301 (2009).
37. Renforth, P. *et al.* Silicate production and availability for mineral carbonation. *Environ. Sci. Technol.* **45**, 2035–2041 (2011).
38. Renforth, P. The negative emission potential of alkaline materials. *Nat. Comms.* **10,** 1401 (2019).
39. Tubana, B.S., Babu, T. & Datnoff, L. E. A review of silicon in soils and plants and its role in US agriculture: history and future perspectives. *Soil Sci.* **181**, 393–411 (2016).
40. Washbourne, C.-L. *et al.* Rapid removal of atmospheric CO_2 in urban soils. *Environ. Sci. Technol.* **49,** 5435-5440 (2015).
41. Lekakh, S.N. *et al.* Kinetics of aqueous leaching and carbonization of steelmaking slag. *Metallurg. Mat. Trans.* **39B,** 125-134 (2008).
42. Haynes, R.J., Belyaeva, O.N. & Kingston, G. Evaluation of industrial waste sources of fertilizer silicon using chemical extractions and plant uptake. *J. Nutr. Soil Sci*., **176,** 238-248 (2013).
43. Rodd, A.V. *et al.* Surface application of cement kiln dust and lime to forage land: effect on forage yield, tissue concentration and accumulation of nutrients. *Can. J. Soil Sci.* **90,** 201-213 (2010).

44. Ramos, C.G. *et al.* Evaluation of soil re-mineralizer from by-product of volcanic rock mining: experimental proof using black oats and maize crops. *Nat. Res. Res.* https://doi.org/10.1007/s11053-019-09529-x (2019).
45. Savant, N.K., Datnoff, L.E. & Snyder, G.H. Depletion of plant-available silicon in soils: A possible cause of declining rice yields. *Comms. Soil Sci. Plant Anal.* **28,** 1245-1252 (1997).
46. Ning, D. *et al.* Impacts of steel-slag-based fertilizer on soil acidity and silicon availability and metals-immobilization in a paddy soil. *PLoS ONE* **11,** e0168163 (2016).
47. Chen, J. Rapid urbanization in China: a real challenge to soil protection and food security. *Catena* **69,** 1-15 (2007).
48. United Nations. *Global land outlook.* First Edition (United Nations Convention to Combat Desertification, Bonn, Germany, 2017).
49. Smith, M.R. & Myers, S.S. Impact of anthropogenic CO_2 emissions on global human nutrition. *Nat. Clim. Change* **8,** 834-839 (2018).
50. Cui, Z. *et al.* Pursuing sustainable productivity with millions of smallholder farmers. *Nature* **555,** 363-366 (2018).
51. Pidgeon, N.F. & Spence, E. (2017) Perceptions of enhanced weathering as a biological negative emissions option. *Biol. Letts*. **13,** 20170024 (2017).
52. Daval, D., Calvarusa, C., Guyut, F. & Turpault, M.-P. Time-dependent feldspar dissolution rates resulting from surface passivation: experimental evidence and geochemical implications. *Earth Plan. Sci. Lett.* **498,** 226-236 (2018).
53. Ricke, K., Drout, L., Caldeira, K. & Tavoni, M. Country-level social cost of carbon. *Nat. Clim. Change* **8,** 895-900 (2018).
54. Cox, E., Pidgeon, N.F., Spence, E.M. & Thomas, G. Blurred lines: The ethics and policy of greenhouse gas removal at scale. *Frontiers Environ. Sci.* https://doi.org/10.3389/fenvs.2018.00038 (2018).

Methods Summary

Carbon removal simulation framework

Our analysis is based on a 1-D vertical reactive transport model for rock weathering with steady-state flow[55,56], and a source term representing rock grain dissolution within the soil profile (SI Methods). The model accounts for changing dissolution rates with soil depth and time as grains dissolve, and chemical inhibition of dissolution as pore fluids approach equilibrium with respect to the reacting basaltic mineral phases, and the formation of pedogenic calcium carbonate mineral in equilibrium with pore fluids. Simulations consider basalts exhibiting relatively slow- versus fast-dissolution rates due to differing mineralogy (SI tables S1-S3). Basaltic minerals undergo dissolution at different rates, with some minerals continuing to undergo dissolution and capture CO_2 after the first year of application. Thus calculating representative annual CO_2 removal rates requires computing average rates derived from repeated basaltic rock dust applications (**Extended Data Fig. 7)**.

Transport equation. The calculated state variable in the transport equation is the dissolved molar equivalents of elements released by stoichiometric dissolution of mineral *i*, in units of mole L^{-1}. ϕ is volumetric water content, C_i is dissolved concentration (mole L^{-1}) of mineral i transferred to solution, t is time (y), q is vertical water flux (m y^{-1}), z is distance along vertical flow path (m), R_i is the weathering rate of basalt mineral i (mole per litre of bulk soil per year) and C_{eq_i} is the solution concentration of weathering product at equilibrium with the mineral phase i (Equation 1).

$$\phi \frac{\partial C_i}{\partial t} = -q \frac{\partial C_i}{\partial z} + R_i \left(1 - \frac{C_i}{C_{eq_i}}\right) \quad (1)$$

Mineral mass balance. The change in mass of basalt mineral i, B_i, is defined by the rate of stoichiometric mass transfer of mineral i elements to solution. Equation 2 is required because we are considering a finite mass of weathering rock, which over time can react to completion, as opposed to *in situ* weathering of the lithosphere, e.g. when considering weathering and geomorphology[56].

$$\frac{\partial B_i}{\partial t} = - R_i \left(1 - \frac{C_i}{C_{eq_i}}\right) \quad (2)$$

Removal of weathering products. The total mass balance over time for basalt mineral weathering allows calculation of the products transported from the soil profile. The total mass of weathering basalt is defined as follows where m is the total number of weathering minerals in the rock, t_f is the duration of weathering (year) and L is the total depth of the soil profile (m).

$$\text{Total weathered Basalt} = \sum_{i=1}^{m} \phi \int_{z=0}^{L} C_i(t,z)\, \mathrm{d}z + q \int_{t=0}^{t_f} C_i(t,L)\, \mathrm{d}t \quad (3)$$

We define q as the net annual sum of water gained through precipitation[57] and irrigation[58], minus crop evapotranspiration[59], as calculated with high spatial resolution gridded datasets (**Extended Data Figs. 8 and 9**; SI Table S14).

Rate law. We modelled application of a crushed fast- or slow-weathering basalt, with specified mineral weight fractions and physical-chemical characteristics (SI Tables S1-S3). Rates of basalt grain weathering define the source term for weathering products and are calculated as a function of soil pH, soil temperature, soil hydrology and crop net primary productivity (NPP) using the linear transition state theory rate law[60-62]. Plant-enhanced basalt weathering is modelled empirically for annual and woody crops with power functions fitted to data (SI fig. S4; SI Table S4). These functions represent the effects of a range of rhizosphere processes that accelerate the physical breakdown and chemical dissolution of minerals, including the activities of nutrient scavenging mycorrhizal fungi that physically disrupt and chemically etch mineral surfaces, and bio-production of low molecular weight organic compounds and chelating agents[63,64].

Soil pH of each grid cell is dynamically calculated from the alkalinity mass and flux balance for an adaptive time-step, controlled by mineral dissolution rates on mineral dissolution, following initialization with a top soil (0-15 cm) pH value based on field data from global soil databases (SI Table S14); soil pH buffering capacity is accounted for with an empirical soil pH buffer function[65]. The soil pCO_2 depth profile of a grid cell is generated with the standard gas diffusion equation[66], scaled by crop NPP × 1.5 to account for combined autotrophic and heterotrophic respiration[67]. The alkalinity balance considers net acidity input during crop growth for biomass-cations removed from the field[68], and secondary mineral precipitation of calcite[18].

Model advances

We incorporate three further significant advances into the above 1-D vertical steady-state flow model. First, we provide a numerical basis for calculating weathering rates using log-normal particle size distributions of basalt grains produced by mechanical crushing and grinding for soil amendment[22,69,70]. This conceptualisation improves on the simplified case of a single mean particle diameter, previously used in ERW calculations[16-18,22,23]. Second, we apply the fractal dimension for surface roughness to relate reacting surface area to basalt mass across physical scales of weathering from the laboratory at which weathering kinetic parameter values are empirically determined to the field at which model results reflect CDR operations[71]. The fractal dimension effectively provides a means of consolidating measurements taken at different scales and accounts for uncertainties in grain topography and porosity[72], and mass transfer rates from rock grains to flowing soil water. Finally, we calculate mean rates of rock dust weathering and CO_2 removal following annual applications by tracking cohorts of particles applied over a 10-year time horizon and their mineral composition (**Extended Data Fig. 7**).

Base-line simulations

Using this modelling framework, we analysed a baseline application rate of 40 t ha^{-1} yr^{-1} (equivalent to a <2 mm layer of rock powder distributed on croplands), which falls within the range of basalt amendments shown to improve crop production in field trials[4]. Net CDR is defined as the difference between CO_2 capture by ERW as dissolved inorganic carbon and soil (pedogenic) carbonate and the sum of CO_2 emissions for logistical operations. Carbon emissions per unit mass of ground rock depend on particle size (**Extended Data Fig. 10**), the

582 CO_2 emissions per kilowatt-hour of electricity generated from component energy sources
583 (fossil fuels, nuclear and renewables), as well as the carbon costs of sourcing and transporting
584 the silicate materials. Rock grinding to reduce particle size and maximise CDR is the
585 primary energy consuming operation in ERW[22,23,73].

586 Assessment of basalt transport from source regions to croplands is based on road and
587 rail network analyses to calculate distances, costs, and carbon emissions for each scenario (SI
588 Methods Section 2.3). Our approach improves on prior analyses, which assumed a fixed
589 radius between rock dust source and site of application[73]. We go beyond global cost
590 estimates[23] by using national fuel (diesel), labour and infrastructure costs to undertake
591 logistical operations, and the price of energy inputs to grind rocks. Our analysis thus
592 represents the first techno-economic assessment in which detailed ERW carbon and
593 economic costs vary within and between nations and account for socio-technical uncertainties
594 in energy production.

595

596 **Carbon dioxide removal**

597 We calculate carbon dioxide removal (CDR) by ERW of crushed basalt applied to soils via
598 two pathways: 1) the transfer of weathered base cations (Ca^{2+}, Mg^{2+}, Na^{+} and K^{+}) from soil
599 drainage waters to surface waters that are charge balanced by the formation of HCO_3^- ions
600 and transported to the ocean (Equation 4), and 2) formation of pedogenic carbonates
601 (Equation 5).

602 Pathway 1 for calcium ions:

603 $$CaSiO_3 + 2CO_2 + 3H_2O \rightarrow Ca^{2+} + 2HCO_3^- + H_4SiO_4 \quad (4)$$

604 Pathway 2 for calcium carbonate formation:

605 $$Ca^{2+} + 2HCO_3^- \rightarrow CaCO_3 + CO_2 + H_2O \quad (5)$$

606 Monovalent and divalent base cations are released from basaltic minerals by dissolution
607 based on stoichiometry (SI Table S2). CDR, via pathway 1, potentially sequesters two moles
608 of CO_2 from the atmosphere per mole of divalent cation. However, ocean carbonate
609 chemistry reduces the efficiency of CO_2 removal (η) to an extent depending on ocean
610 temperature, salinity and the surface ocean dissolved CO_2 concentration. We calculate η for
611 average ocean temperature (17 °C), salinity (35%) and an RCP8.5 2050 dissolved pCO_2 of
612 600 μatm, giving $\eta = 0.86$, i.e., 0.86 mole of CO_2 removal per mole of monovalent cation and
613 1.72 mol of CO_2 removed per mol of divalent cation added to the oceans[20]. For Pathway 1,
614 the efficiency of CDR = $\eta \times \sum$(mol monovalent cations)+$2\eta \times \sum$(mol divalent cations).

615 CDR via pathway 2 can occur if dissolved inorganic carbon derived from atmospheric
616 CO_2 precipitates as pedogenic carbonate, and sequesters 1 mol of CO_2 per mole of Ca^{2+}
617 instead of 1.72 mol of CO_2 via pathway 2 and is therefore less efficient. Thus for any given
618 grid cell, we compute CO_2 removal by ERW as the alkalinity flux in soil drainage and
619 pedogenic calcite precipitation. Possible CO_2 degassing due to changes in surface water
620 chemistry during transport in large river systems[74] is not considered.

621

622 **Cost assessment modelling**

623 An overview of the environmental costs model and its linkages with the performance model
624 is presented in **Extended Data Fig. 4**. We include contributions to total cost of 1) mining, 2)
625 processing[75,76], 3) distribution and transport and 4) spreading on agricultural land. We
626 considered how the cost of energy and the carbon emissions varied with grinding to different

particle size distributions (**Extended Data Fig. 10**). Grinding to finer particles requires greater energy and results in higher carbon emissions. We defined the particle size distribution by the *p*80 value; i.e. 80% of the particle mass with less than or equal to a specified particle size. We calculated the optimized *p*80 that results in maximum net CDR for each grid cell and this was conducted for different fractions of a country's crop area (0.1 to 1.0 at 0.1 increments), ordered according to weathering potential. For a given *p*80 value, we calculate the weathering rate for each grid cell, sort them in descending order and find the grid cells that comprise the cumulative area fraction for each increment.

Optimization is conducted for each combination of the two types of basalt and the two quasi-log-normal particle size distributions for each country (SI Tables S1-S3). Country-specific electricity production and the forecast fractional contributions to electricity production by different energy sources (coal, natural gas, oil, solar PV, concentrated solar power, hydropower, wind, marine) for 2050 are based on business-as-usual (BAU), i.e., currently implemented energy polices, and energy projections consistent with a 2°C (2°C) warming scenario (**Extended Data Fig. 9**)[5]. National CO_2 emissions for electricity generation consistent with both scenarios were based on results reported in Ref[5] (SI Tables S6-S9). Industrialized nations (e.g., Canada) consume up to ~2% of their total energy production on rock comminution (crushing and grinding) processes[77]. We assume a future maximum upper limit of 3% energy consumption for all nations, based on the rationale that current rates for developed nations grow from around 2% today in-line with national projected energy production[5] in 2050 (**Extended Data Fig. 2**).

Distribution costs and emissions were calculated by performing spatial analysis with ArcGIS software. Basalt rock sources were identified from the GLiM rock database[78], excluding those in protected areas[79]. We then performed a global transport (rail and road) network analysis by modelling a logistic ERW supply by creating an Origin-Destination Cost Matrix using GIS[80,81]. For larger datasets, the Origin-Destination cost matrix searches and measures the least-cost paths along the network from multiple origins to multiple destinations to identify the most cost-effective or shortest route between a source and destination. Transport analyses used the lowest emission option between rail and road network to calculate distribution costs and CO_2 emissions (SI Tables S10-S12). Freight-rail emissions were obtained from 2050 projections of reduced carbon emissions following improvements in energy efficiency[82]. Rail CO_2 emissions were the same for both the business-as-usual (BAU) and 2°C scenarios. For road transport, we considered estimated energy consumption of currently/shortly available heavy electric trucks 1.38 (kWh/km)[83] and projected carbon emissions in the electricity sector of each country for BAU or the 2°C scenario[5].

Forecasting bulk silicate waste production

We developed a model that relates global per capita material production (for cement) or consumption (steel) *P* to per capita gross world product (*GWP*)[84,85] through historical global data using nonlinear least squares (Equation 6).

$$P = ae^{-b/GWP} \qquad (6)$$

where *a* and *b* are regression constants. The derived saturation value, *a*, was used in a further regression through national data normalised to 2014 production and GDP (Equation 7).

$$P = P_{REF} \times (1 + \big((m + r) \times \Delta GDP\big) \times e^{(a \times \left(1 - e^{-(m \times \Delta GDP)}\right)) - (m \times \Delta GDP)} \qquad (7)$$

where P_{REF} is the global per capita consumption in a given reference year (2014), ΔGDP is the deviation of the per capita gross domestic product from the reference year, and *m* and *r*

673 are regression constants. These results were used together with averaged projections of
674 future GDP (SI Table S14) from the 'middle-of-the-road' Shared Socioeconomic Pathway
675 (SSP2) to derive nationally resolved projections of future per capita
676 consumption/production[85]. SSP2 potentially represents the largest material production
677 pathway, as other SSPs forecast lower consumption or economic growth producing 30-50%
678 less material globally. We have not considered the penetration of recycling into steel
679 production beyond its current rate. Cement and cement kiln dust have no capacity to be
680 recycled as cement. The total production/consumption at a given time, $T(t)$, was calculated by
681 multiplying the population, $Pop(t)$, by production or consumption (P). We assume 115 kg of
682 cement kiln dust is produced as a by-product in kilns for every tonne of clinker, and have
683 modelled the production of demolition waste following an average 50-year service life
684 (normally distributed with a standard deviation of 10 years)[86]. The ratio of pig iron to steel
685 production (0.72) was obtained using linear regression of 1960-2014 data, negating the need
686 to explicitly model pig iron displacement from scrap recycling, and assuming the scrap ratio
687 remains unchanged. All steel and blast furnace slag was considered available for reaction
688 with CO_2. Between 2006–2014, 185 kg of blast furnace slag and 117 kg of steel slag was
689 produced for every tonne of crude steel[87].

690

691 **Data availability**

692 Datasets on global crop production and yield are available at: http://www.earthstat.org/, accessed on
693 18/12/2019

694 Datasets on global crop evapotranspiration are available at: https://www.uni-
695 frankfurt.de/45217988/Global_Crop_Water_Model__GCWM, accessed on 18/12/2019

696 Datasets on global crop irrigation are available at: https://zenodo.org/record/1209296, accessed on
697 accessed 18/12/2019

698 Datasets on global precipitation are available at: http://www.climatologylab.org/terraclimate.html,
699 accessed on 18/12/2019

700 Datasets on global soil surface pH are available at: https://daac.ornl.gov/SOILS/guides/HWSD.html,
701 accessed on 18/12/2019

702 Datasets on global soil temperature are available at: https://esgf-node.llnl.gov/search/cmip5/, accessed
703 on 18/12/2019

704 Datasets on diesel prices are available at https://data.worldbank.org/indicator/EP.PMP.DESL.CD

705 Datasets on mining costs are available at http://www.infomine.com/

706 Datasets on gross national income per capita are available at
707 https://data.worldbank.org/indicator/ny.gnp.pcap.pp.cd

708 Datasets for projections of future GDP linked to Shared Socioeconomic Pathways are available at:
709 https://tntcat.iiasa.ac.at/SspDb

710

711 **Source data**

712 Source Data for figures 1 to 4 are available from nature.com [please insert web location of the
713 uploaded datasets].

714 **Code availability**

715 The Matlab codes developed for this study belong to the Leverhulme Centre for Climate Change
716 Mitigation. We will make them available upon reasonable request.

717

55. Berner, R.A. Rate control of mineral dissolution under earth surface conditions. *Am. J. Sci.* **278,** 1235–1252 (1978).
56. Maher, K. The dependence of chemical weathering rates on fluid residence time. *Earth Plan. Sci. Lett.* **294,** 101-110 (2010).
57. Abatzoglou, J.T., Dobrowski, S.Z., Parks, S.A. & Hegewisch, K.C. TerraClimate, a high-resolution global dataset of monthly climate and climatic water balance from 1958-2015. *Sci. Data,* **5,** 170191 (2018).
58. Huang, Z.W. *et al.* Reconstruction of global gridded monthly sectoral water withdrawals for 1971-2010 and analysis of their spatiotemporal patterns. *Hydrol. Earth Syst. Sci.* **22,** 2117-2133 (2018).
59. Siebert, S. & Doll, P. Quantifying blue and green virtual water contents in global crop production as well as potential production losses without irrigation. *J. Hydrol.* **384,** 198-217 (2010).
60. Aagaard, P. & Helgeson, H. C. Thermodynamic and kinetic constraints on reaction-rates among minerals and aqueous-solutions. 1. Theoretical considerations. *Am J Sci* **282**, 237-285, (1982).
61. Lasaga, A. C. Chemical-kinetics of water-rock interactions. *J. Geophys. Res.* **89**, 4009-4025 (1984).
62. Brantley, S.L., Kubicki, J.D. & White, A.F. *Kinetics of water-rock interaction* (Springer, New York, 2008).
63. Harley, A.D. & Gilkes, R.J. Factors influencing the release of plant nutrient elements from silicate rock powders: a geochemical overview. *Nutr. Cycl. Agroecosys.* **56,** 11-36 (2000).
64. Taylor, L.L. *et al.* Biological evolution and the long-term carbon cycle: integrating mycorrhizal evolution and function into the current paradigm. *Geobiology*, **7,** 171-191 (2009).
65. Nelson, P.N. & Su, N. Soil pH buffering capacity: a descriptive function and its application to some acidic tropical soils. *Aust. J. Soil Sci.* **48,** 201-207 (2010).
66. Cerling, T. Carbon dioxide in the atmosphere: evidence from Cenozoic and Mesozoic paleosols. *Am. J. Sci.*, **291**, 377–400 (1991).
67. Taylor, L., Banwart, S.A., Leake, J.R. & Beerling, D.J. Modelling the evolutionary rise of ectomycorrhizal on sub-surface weathering environments and the geochemical carbon cycle. *Am. J. Sci.*, **311**, 369–403 (1991).
68. Banwart, S.A., Berg, A. & Beerling, D.J. Process-based modelling of silicate mineral weathering responses to increasing atmospheric CO_2 and climate change. *Global Biogeochem. Cycles*, **23,** GB4013.
69. Petavratzi, E., Kingman, S. & Lowndes, I. Particulates from mining operations: A review of sources, effects and regulations. *Miner Eng* **18**, 1183-1199, doi:10.1016/j.mineng.2005.06.017 (2005).
70. Cepuritis, R., Garboczi, E. J., Ferraris, C. F., Jacobsen, S. & Sorensen, B. E. Measurement of particle size distribution and specific surface area for crushed concrete aggregate fines. *Adv Powder Technol* **28**, 706-720, doi:10.1016/j.apt.2016.11.018 (2017).
71. Navarre-Sitchler, A. & Brantley, S. Basalt weathering across scales. *Earth Plan Sci. Lett.* **261,** 321-334 (2007).
72. Brantley, S. L. & Mellott, N.P. Surface area and porosity of primary silicate minerals. *Am Mineral* **85**, 1767-1783 (2000).
73. Moosdorf, N., Renforth, P. & Hartmann, J. Carbon dioxide efficiency of terrestrial weathering. *Environ. Sci. Tech.* **48**, 4809–4816 (2014).
74. Salisbury, J.E. *et al.* Seasonal observations of surface waters in two Gulf of Maine estuary-plume systems: Relationships between watershed attributes, optical measurements and surface pCO_2. *Estuarine, Coast. Shelf Sci.* **77,** 245–252 (2008).
75. Darling, P. & Society for Mining Metallurgy and Exploration (U.S.). *SME mining engineering handbook*. 3rd edn (Society for Mining, Metallurgy, and Exploration, 2011).
76. InfoMine. *InfoMine, Mining Cost Service*, http://www.infomine.com/ (2009).
77. Tromans, D. Mineral comminution: energy efficiency considerations. *Min. Engin.* **21,** 613-620 (2008).
78. Hartmann, J. & Moosdorf, N. The new global lithological map database GLiM: A representation of rock properties at the Earth surface. *Geochem Geophy Geosy* **13**, doi:Artn Q1200410.1029/2012gc004370 (2012).

79. UNEP-WCMC and IUCN (2018), *Protected Planet: The World Database on Protected Areas* (WDPA)/The Global Database on Protected Areas Management Effectiveness (GD-PAME)] (Cambridge, UK: UNEP-WCMC and IUCN 2018).
80. ROTARU, A. S. *et al.* Modelling a Logistic Problem by Creating an Origin-Destination Cost Matrix using GIS Technology. *Bulletin UASVM Horticulture*, **71,** (2014).
81. Osorio, C. Dynamic origin-destination matrix calibration for large-scale network simulators. *Transportation Research Part C: Emerging Technologies* **98**, 186-206 (2019).
82. International Energy Agency. *The Future of Rail, Opportunities for energy and the environment* (International Energy Agency, Paris, France, 2019).
83. Liimatainen, H., van Vliet, O. & Aplyn, D. The potential of electric trucks – an international commodity-level analysis. *App. Energy*. 236, 804-814 (2019).
84. The World Bank. *GDP (current US$)*, https://data.worldbank.org/indicator/NY.GDP.MKTP.CD (2016).
85. Bauer, N. *et al.* Shared socio-economic pathways of the energy sector – quantifying the narratives. *Glob. Environ. Change* **42,** 316-330 (2017).
(available at https://tntcat.iiasa.ac.at/SspDb)
86. Xi, F. *et al.* Substantial global carbon uptake by cement carbonation. *Nat. Geosci.* **9,** 880-883 (2016).
87. U.S. Geological Survey. *Mineral Commodity Summaries 2006*. (US Geological Survey, Washington, USA, 2006).

Acknowledgements. We thank Adisa Azapagic and John Shepherd for helpful comments on an earlier draft, and acknowledge discussions with additional members of the Royal Society-Royal Academy of Engineering Greenhouse Gas Removal Working Group. We gratefully acknowledge funding of this research with a Leverhulme Research Centre Award (RC-2015-029) from the Leverhulme Trust. Lyla Taylor is thanked for advice and discussions during model development and Joe Quick provided data and analysis on plant weathering. P.R. acknowledges UKRI funding under the UK Greenhouse Gas Removal Programme (NE/P019943/1, NE/P019730/1); I.A.J. acknowledges the financial support from the Research Council of the University of Antwerp. We acknowledge the World Climate Research Programme's Working Group on Coupled Modelling responsible for CMIP and thank the climate modelling groups for producing and making available their model output. For CMIP the US Department of Energy's Program for Climate Model Diagnosis and Intercomparison provides coordinating support and led development of software infrastructure in partnership with the Global Organization for Earth System Science Portals.

Author contributions. D.J.B., E.P.K., M.R.L., P.W., S.Q. and S.A.B. designed the study, E.P.K. and M.R.L. undertook model development and coding, with input from P.W., S.A.B., S.Q. and D.J.B. E.P.K. undertook data analysis and synthesis, R.M.E. and L.K. undertook the GIS transport analyses, P.R. the silicate production modelling, and N.P. wrote sections on public perception. J.-F.M., H.P., N.R.E. and P.B.H. provided data on national energy production and sources, and CO_2 emissions for both scenarios. M.G.A., R.H.J., C.R.P., M.K., B.S. and I.A.J. all provided input on sections and addition of appropriate references specific to their area of expertise. D.J.B. and S.A.B. wrote the manuscript, with input from J.H.

Competing Interests. The authors declare no competing interests.

Supplementary Information.
This file contains Methods, Figures S1 to S25, Tables S1 to S15, and References.

Correspondence and requests for materials should be addressed to D.J.B.

Peer review information.

Reprints and permissions information is available at www.nature.com/reprints.

Figure legends

Fig. 1 | Carbon removal via enhanced rock weathering with croplands. Net carbon dioxide removal (CDR) curves for nations with the highest CDR potential worldwide (**a-g**) and in Europe (**h-l**) as a function of increasing enhanced rock weathering deployment across existing croplands. Note y-axis scale changes. Results are shown for the business-as-usual (BAU) and the 2°C energy policy scenarios. Grey shaded area for each nation represents the 90% confidence interval calculated for basalts with relatively slow- versus fast-weathering rates for the BAU scenario; short green dashed lines indicate the 90% confidence limits of the corresponding 2°C scenario simulations. Uncertainty in net CDR increases as ERW deploys onto croplands occupying a wider range of environmental conditions.

Fig. 2 | Augmentation of pledged CO_2 emissions reduction by enhanced rock weathering. Fraction of 2030 national determined carbon (NDC) emissions reductions by enhanced weathering for nations with the highest CDR potential worldwide (**a-g**) and in Europe (**h-l**), as a function of increasing enhanced rock weathering deployment across croplands. Note y-axis scale changes. Results are shown for the business-as-usual (BAU) energy policy and the 2°C energy policy scenarios. Grey shaded area for each nation represents the 90% confidence interval calculated for basalts with relatively slow- versus fast-weathering rates for the BAU scenario; short green dashed lines indicate the 90% confidence limits of the corresponding 2°C scenario simulations.

Fig. 3 | Costs of carbon extraction via enhanced rock weathering with croplands. Costs of CO_2 extraction from air by ERW for nations with the highest CDR potential worldwide (**a-g**) and in Europe (**h-l**), as a function of increasing enhanced rock weathering deployment across croplands. Results are shown for the business-as-usual (BAU) and the 2°C energy policy scenarios. Grey shaded area for each nation represents the 90% confidence interval calculated for basalts with relatively slow- versus fast-weathering rates for the BAU scenario; short green dashed lines indicate the 90% confidence limits of the corresponding 2°C scenario simulations.

Fig. 4 | Forecast increases in national bulk silicate production over the next century. Simulated future increases in bulk artificial silicate by products (slag, cement, kiln dust, and cementitious demolition waste) production during the 21st Century are given for (**a**) China, (**b**) India, (**c**) USA and (**d**) Brazil. Based on the middle-of-the-road Shared Socioeconomic Pathway (Methods).

Extended Data Figure legends

Extended Data Fig. 1 | Performance model schematic. Detailed methods are provided in SI Methods, Sections 1-2. Spatially resolved key drivers are mapped in Extended Data Fig. 8; sources given in SI Table S14.

Extended Data Fig. 2 | Cumulative energy demand for rock grinding by nation. Results are shown for the top seven nations of the world (**a**) to (**g**), and the top five European nations (**h**) to (**l**), as ranked by net CO_2 removal capacity, with increasing fractional cropland area of enhanced rock weathering deployment. Curves depict simulations for the business as usual (BAU) and 2°C energy policy scenarios. Grey shaded area for each nation represents the 90% confidence interval calculated for basalts with relatively slow- versus fast-weathering rates for the BAU scenario; short green dashed lines indicate the 90% confidence limits of the corresponding 2°C scenario simulations.

Extended Data Fig. 3 | Simulated net CO_2 removal with croplands via enhanced rock weathering. Net rates of CO_2 sequestration on croplands (annual and perennial combined) for the four target global CO_2 removal rates, 0.5, 1.0, 1.5 and 2.0 Gt CO_2 yr^{-1} (Table 1) for the business-as-usual (BAU) (**a**) to (**d**) and the 2°C (**e**) to (**h**) energy policy scenarios.

Extended Data Fig. 4 | Schematic overview of the environmental economics model. Interactions are shown between the performance model, calculating net CO_2 removal, and the major components of the environmental economic model. Spatially resolved key drivers are mapped in Extended Data Fig. 9; sources given in SI Table S14.

Extended Data Fig. 5 | Cumulative silicate demand by nation. Results are shown for the top seven nations of the world (**a**) to (**g**), and the top five European nations (**h**) to (**l**), as ranked by net CO_2 removal capacity, with increasing fractional cropland area deployment of enhanced rock weathering. Note y-axis scale changes for European countries. Curves are the same irrespective of energy policy scenario.

Extended Data Fig. 6 | Secondary CO_2 emissions from logistical enhanced rock weathering operations in 2050. Results are shown for (**a**) the top seven nations of the world and (**b**) the top five European nations for the business-as-usual (BAU) and for the same groupings in (**c**) and (**d**) for the 2 °C energy policy scenarios. For each country, bars from left to right, are for a 0.25, 0.5, 0.75 and 1.0 fraction of ERW deployment on croplands. Under the BAU scenario, CO_2 emissions from grinding dominate secondary emissions associated with ERW, except for France where low carbon nuclear power dominates. Under the 2°C energy policy scenario, (**c**) and (**d**), secondary CO_2 emisssion generally drop for most nations as they transition to low carbon energy sources in 2050 and implement negative emissions.

Extended Data Fig. 7 | Multi-year performance model simulations of weathering. Illustrative multi-year simulations of annual basalt application with the performance model showing the effects on soil pH, average efficiency of CO_2 removal (RCO_2), and soil mineral masses over a 10-year time horizon. (**a**) - (**c**) denote pH, RCO_2 and mineral mass results for the tholeiitic basalt, respectively and (**d**) to (**f**) results of the same quantities for the alkali basalt (SI Tables S1-S3). All simulations used the same *p*80 particle size (100 μm) and were undertaken at 20 °C. Multi-year simulations capture the effect of basaltic minerals undergoing dissolution at different rates, with some minerals continuing to undergo dissolution and capture CO_2 after the first year of application. It allows computing average rates of weathering and CO_2 removal from repeated basaltic rock dust applications. Our extended theory underpinning our simulation framework tracks cohorts of particles applied each year and their mineral composition over time to account for cumulative effects (SI Methods).

Extended Data Fig. 8 | Spatially resolved drivers of the performance model. (**a**) soil temperature from the HadGEM RCP8.5 simulation for 2050, (**b**) HYDE harmonized soil pH database, (**c**) annual cropland soil water infiltration (irrigation water + precipitation minus evapotranspiration), (**d**) and (**e**) net primary production index for annual and perennial crops as derived from FAO datasets, respectively. Data sources and spatial resolution are specified in SI Table S14.

Extended Data Fig. 9 | Spatially resolved drivers for environmental economics modelling. (**a**) Industrial diesel prices (US dollar, USD), CO_2 emissions intensity for (**b**) the business-as-usual scenario (BAU), and (**c**) the 2 °C scenario, (**d**) gross national income per capita and (e) industrial electricity prices (US dollar, USD). Data sources and spatial resolution are specified in SI Table S14.

Extended Data Fig. 10 | Relationship between particle size, surface area and grinding energy. (a) Relationship between particle size and surface area, (**b**) surface area and grinding energy and (**c**) particle size and grinding energy, where *p*80 is defined as 80% of the particles having a diameter less than or equal to the specified size. Derived from data in Ref[73].

Table 1. Carbon dioxide removal (CDR) targets for enhanced weathering with croplands in 2050. Relative contribution of each nation is determined by their peak CDR capacity*. Values are means of both energy scenarios; see main text for details.

Target		Cropland area (%)	National CDR (Gt CO_2 yr^{-1})	Silicate demand (Gt yr^{-1})	Cost (US$ t CO_2^{-1} yr^{-1})
0.5 Gt CO_2 yr^{-1}					
World	China	10	0.13	0.77	102.1
	USA	11	0.11	0.63	160.3
	India	11	0.15	0.84	78.4
	Brazil	10	0.041	0.22	123.8
	Indonesia	10	0.017	0.091	54.3
	Canada	10	0.022	0.13	177.6
	Mexico	10	0.013	0.073	97.5
Europe	France	10	0.017	0.085	158.1
	Germany	11	0.012	0.066	167.8
	Italy	11	0.0070	0.039	181.9
	Spain	10	0.012	0.066	192.8
	Poland	10	0.0085	0.050	171.6
1.0 Gt CO_2 yr^{-1}					
World	China	23	0.26	1.59	109.3
	USA	24	0.21	1.26	168.5
	India	23	0.24	1.50	79.9
	Brazil	23	0.083	0.45	116.4
	Indonesia	25	0.033	0.18	57.5
	Canada	16	0.030	0.20	191.7
	Mexico	23	0.025	0.15	103.1
Europe	France	24	0.034	0.17	160.4
	Germany	25	0.025	0.14	171.7
	Italy	23	0.014	0.083	191.0
	Spain	17	0.018	0.10	190.9
	Poland	17	0.012	0.081	170.9
1.5 Gt CO_2 yr^{-1}					
World	China	38	0.40	2.48	114.5
	USA	39	0.32	1.99	173.1
	India	36	0.37	2.35	80.2
	Brazil	36	0.13	0.71	110.5
	Indonesia	41	0.050	0.28	58.6
	Canada	25	0.045	0.35	207.3
	Mexico	37	0.038	0.23	105.6
Europe	France	38	0.050	0.26	159.5
	Germany	39	0.037	0.20	173.6
	Italy	37	0.021	0.13	194.1
	Spain	28	0.026	0.17	189.3
	Poland	27	0.019	0.13	171.3
2.0 Gt CO_2 yr^{-1}					
World	China	55	0.53	3.46	120.7
	USA	55	0.42	2.72	176.7
	India	51	0.49	3.30	80.9
	Brazil	51	0.17	0.98	106.2
	Indonesia	59	0.067	0.38	59.4
	Canada	35	0.060	0.51	220.3
	Mexico	52	0.050	0.33	106.8
Europe	France	54	0.067	0.36	157.1
	Germany	57	0.050	0.28	175.9
	Italy	55	0.029	0.18	193.3
	Spain	41	0.035	0.25	190.7
	Poland	38	0.025	0.19	175.4

*For each country i, we assigned its contribution to a CDR target as below; CDR_{MAX} is the maximum CDR value attainable by a country: $CDR_{Contr}(i) = CDR_{Target} \frac{CDR_{MAX}(i)}{\sum_{j=1}^{Countries} CDR_{MAX}(j)}$

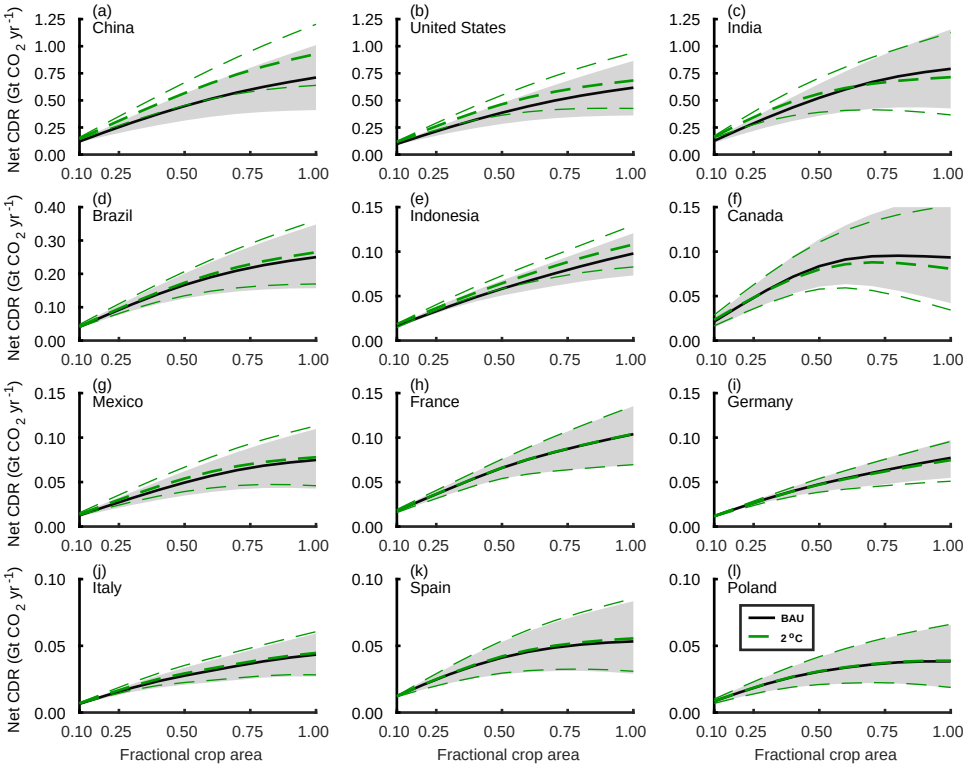
(a)
China
(b)
United States
(c)
India
(d)
Brazil
(e)
Indonesia
(f)
Canada
(g)
Mexico
(h)
France
(i)
Germany
(j)
Italy
(k)
Spain
(l)
Poland
BAU
2 °C
Net CDR (Gt CO 2 yr-1)
Fractional crop area
0.10 0.25 0.50 0.75 1.00

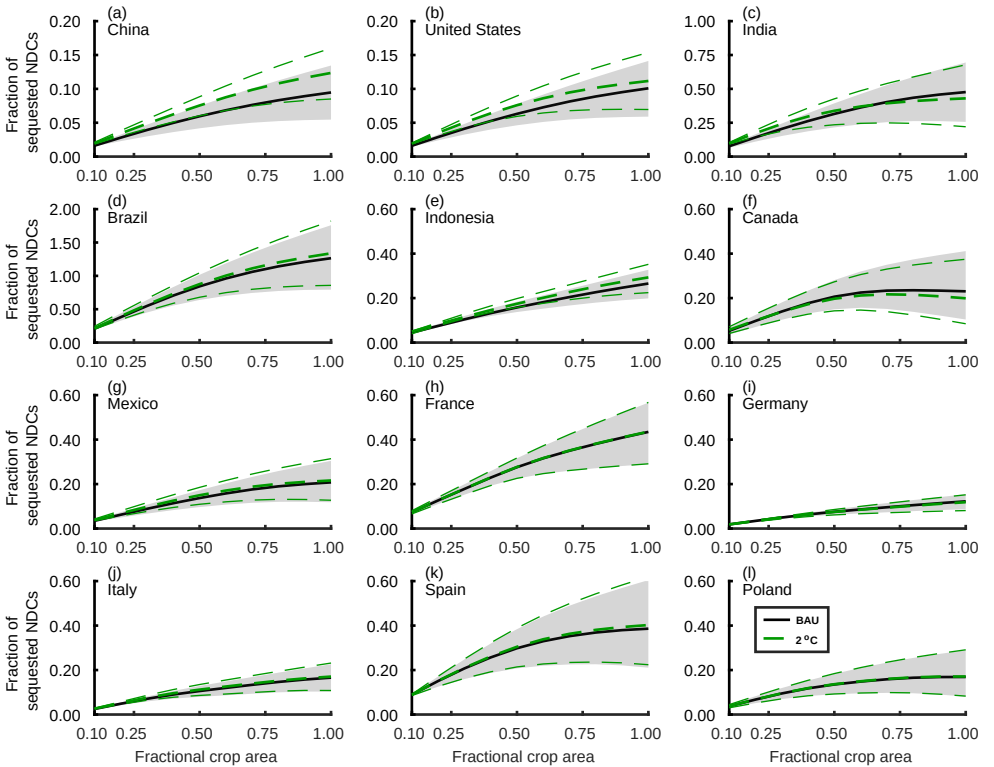
(a)
China
(b)
United States
(c)
India
(d)
Brazil
(e)
Indonesia
(f)
Canada
(g)
Mexico
(h)
France
(i)
Germany
(j)
Italy
(k)
Spain
(l)
Poland
BAU
2 °C
Fraction of sequested NDCs
Fractional crop area
0.10 0.25 0.50 0.75 1.00

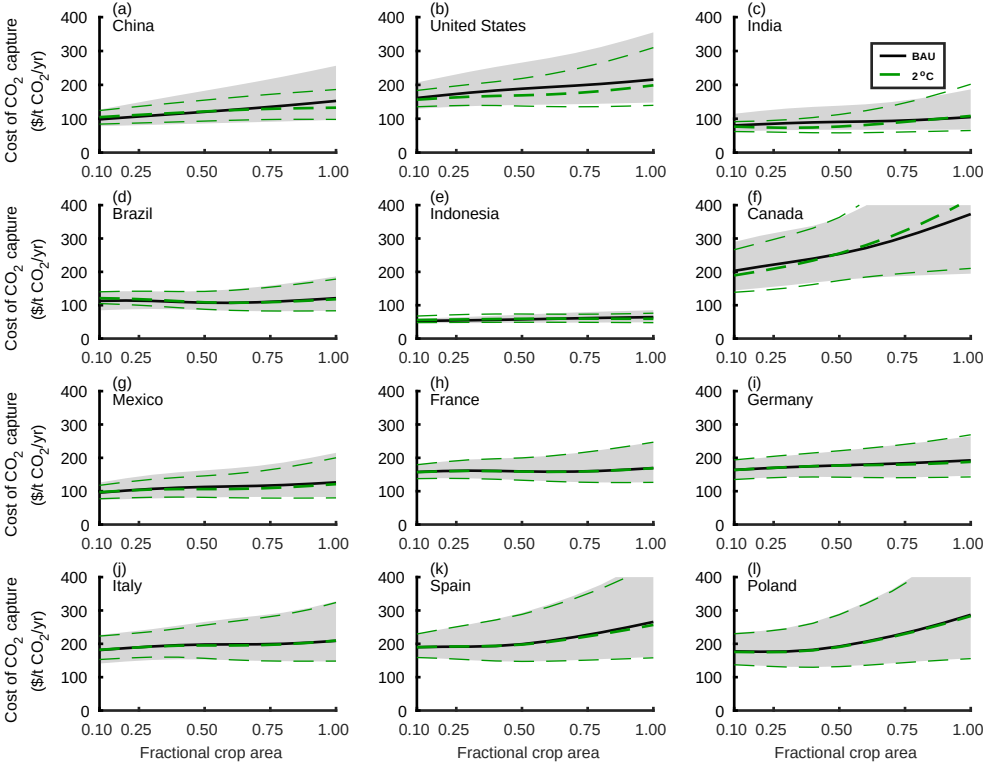
(a)
China
(b)
United States
(c)
India
(d)
Brazil
(e)
Indonesia
(f)
Canada
(g)
Mexico
(h)
France
(i)
Germany
(j)
Italy
(k)
Spain
(l)
Poland
BAU
2 °C
Cost of CO2 capture ($/t CO2/yr)
Fractional crop area
0
100
200
300
400
0.10
0.25
0.50
0.75
1.00

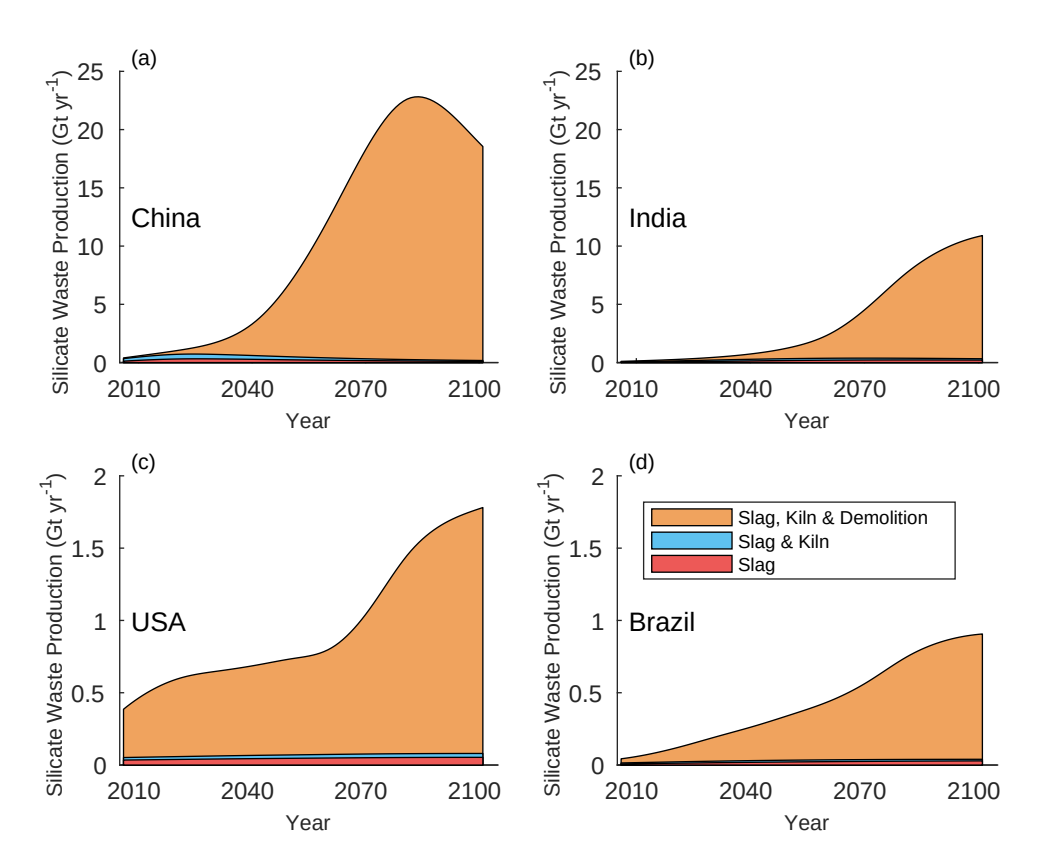
(a)
China
Silicate Waste Production (Gt yr-1)
25
20
15
10
5
0
2010
2040
2070
2100
Year
(b)
India
Silicate Waste Production (Gt yr-1)
25
20
15
10
5
0
2010
2040
2070
2100
Year
(c)
USA
Silicate Waste Production (Gt yr-1)
2
1.5
1
0.5
0
2010
2040
2070
2100
Year
(d)
Brazil
Slag, Kiln & Demolition
Slag & Kiln
Slag
Silicate Waste Production (Gt yr-1)
2
1.5
1
0.5
0
2010
2040
2070
2100
Year